

Accounts

Observation of Coherent Recurrence Motion of Excitons in Anthracene Dimers

Iwao Yamazaki,* Seiji Akimoto, Naoki Aratani,[1] and Atsuhiro Osuka[1]

Department of Molecular Chemistry, Graduate School of Engineering, Hokkaido University, Sapporo 060-8628

[1]Department of Chemistry, Graduate School of Science, Kyoto University, Kyoto 606-8502

Received July 5, 2004; E-mail: yamiw@eng.hokudai.ac.jp

Intramolecular electronic excitation transfer in anthracene dimers in solution at room temperature has been investigated by probing the fluorescence anisotropy decay with a femtosecond up-conversion method. Two types of anthracene dimers were used: anthracenophane (DTA) in which two anthracene rings are stacked parallel, but with nearly orthogonal orientation, and two dianthrylbenzenes (*m*- and *o*-DAB) in which two anthracene rings are linked to a benzene ring at *meta*- and *ortho*-positions. There appeared damped oscillations of apparent periods of 0.6–1.0 ps and damping time constants of 0.7–1.2 ps. The ordinary fluorescence decay (excited-state population decay) obtained with the magic angle excitation exhibits no oscillation in all the cases. It has been found from a theoretical analysis that the oscillatory behaviors on fluorescence anisotropy are consistent with the coherent recurrence motion of an exciton between two anthracene moieties. The magnitudes of the dipole–dipole energy transfer interaction are estimated to be 10–80 cm^{-1}, which are considerably smaller than the experimental value (30–100 cm^{-1}) deduced from the angular frequencies of oscillation. This means that some interchromophore interaction other than the dipole–dipole resonance interaction is involved in the energy transfer interaction in strongly coupled dimers. The longer dephasing time can be explained as a consequence of rigid dimeric conformations in anthracene dimers.

Recent progress of organic synthesis research has provided us with various kinds of supramolecular systems with important features of photophysical and photochemical responses. In our recent studies of porphyrin arrays and porphyrin dendrimers, we found that the intramolecular electronic excitation transfer occurs from an outer-surface donor to the inner-core acceptor on the time scale of ~1 ps or less.[1–3] It is to be noted that a direct energy transfer from the S_2 states of donor plays a more important role than the ordinary transfer process from a thermally equilibrated S_1 state. Furthermore, the reaction rate is larger than or comparable to those of the intramolecular energy relaxation processes such as the vibrational relaxation (VR), the internal conversion (IC), and the internal vibrational redistribution (IVR). Such ultrafast and non-equilibrium excitation transports are associated with fairly strong energy transfer interactions ($\beta = 10$–50 cm^{-1}) in a pair of an excited donor and an acceptor incorporated in a supramolecular framework. Such transports make a striking contrast to many cases of the ordinary energy transfer processes ($\beta < 1$ cm^{-1}) between randomly dispersed molecules in solution.

In cases of the ordinary energy transfer under weak interaction, the reaction is characterized by an irreversible reaction which occurs according to Fermi's golden rule, and the reaction mechanism can be formulated as Förster's *very weak coupling case*.[4] On the other hand, a stronger interaction may occur as the reversible motion of an exciton wave packet through a molecular system. This type of reaction is known as Förster's *intermediate* or *strong coupling case*.[4] If the quantum mechanical phase of the reaction in an ensemble is preserved during the reaction, in other words, if the reaction is completed before the quantum coherence is lost, the energy transfer process could be observed as the recurrence motion of an exciton wavepacket by the use of a time-dependent spectroscopy with sufficiently high time resolution. In fact, such coherent processes can be observed in the excitation energy transfer in photosynthetic light-harvesting antenna proteins where many Bchl *a* molecules are arranged in a space with highly specific structures.[5,6] In the vertically oriented ring inside a LH2 protein complex, an excitation energy propagates coherently around the ring structure as a quantum wavepacket of the exciton. The quantum beat phenomenon was observed with a time period of 100–200 fs. Also, for the primary step of the charge separation in the special dimer, a similar damped oscillation is seen.[7] These oscillatory behaviors indicate that the energy transfers and electron transfers in highly organized molecular systems can occur as coherent processes even in condensed phase at room temperature.

For artificial molecular systems particularly for the bichromophoric molecules as shown in Fig. 1 in which two identical chromophores are connected closely to form a stronger interac-

Published on the web November 11, 2004; DOI 10.1246/bcsj.77.1959

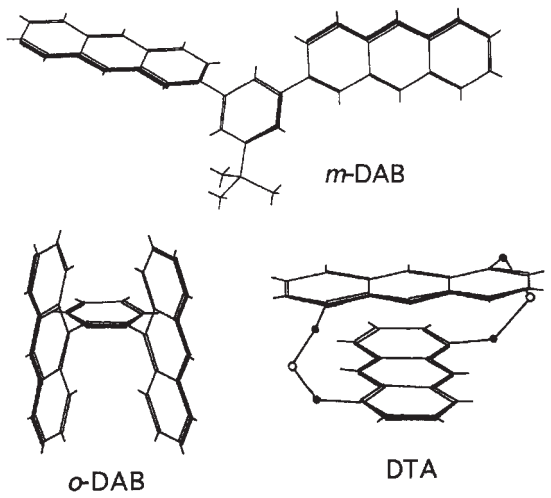

Fig. 1. Molecular structures of anthracene dimers (*m*-DAB and *o*-DAB) and dithiaanthracenophane (DTA) concerned in the present study.

tion, the quantum mechanical theory predicts that the interchromophore energy transfer will occur via recurrence motion of excitation between the two chromophores. Following photoexciting coherently the "exciton" states, i.e., the superposition states of two locally excited states which are split by an interaction energy 2β, the local excitation moves back and forth between the two coupled chromophores. The recurrence motion of exciton could be observed, in principle, with a time-dependent fluorescence anisotropy measurement based on the photoselection method. However, such a predicted phenomenon is essentially difficult to observe experimentally because of very fast randomization (dephasing) of the exciton wavepacket in an ensemble. To observe such a recurrence experimentally through a fluorescence anisotropy decay, one must employ the following experimental conditions; (1) the spectral coherence of excitation light pulse must be broad enough to span the two eigenstates so that the off-diagonal density matrix elements may become populated and therefore select localized states; (2) the time period of the coherent oscillation should be shorter than the electronic dephasing time; (3) the lab frame orientation of the electronic transition moments of absorption or emission is different between the different halves of bichromophore system. Under such conditions (1)–(3), the recurrence motion of an exciton may appear as a damped oscillation on the fluorescence anisotropy decay, which is defined as the intensity difference of the probe signals parallel ($I_{\parallel}$) and perpendicular ($I_{\perp}$) to the polarization plane of the excitation laser divided by the omni-directional signal ($I_{\parallel} + 2I_{\perp}$), i.e., $r(t) = (I_{\parallel} - I_{\perp})/(I_{\parallel} + 2I_{\perp})$.

Whether or not such a predicted macroscopic quantum coherence is observable depends on the strength of the coupling of the exciton to the heat bath. In fact, theoretical studies on the energy transfer between two coupled chromophores predicted that the initial electronic coherence and the dephasing path which randomize the quantum mechanical phase have sensitive effects on the fluorescence anisotropy. Rahman et al.[8] and Knox and Gülen[9] treated this problem theoretically on the basis of the stochastic Liouville equation using the density matrix. They demonstrated that the initial value of the anisotropy is larger than 0.4, i.e., the anisotropy value usually observed for a collection of randomly oriented molecules. Matro and Cina[10] calculated the time course of the fluorescence anisotropy based on the Redfield theory, and demonstrated an important role of vibronic transitions. Fujimura et al.[11] presented an oscillating profile of the excited-state population in two coupled molecules by a model calculation using Liouville equation. From these theoretical predictions, one can expect to observe the electronic coherence or the recurrence dynamics of energy transfer if one uses molecular systems of suitably designed arrangements of chromophores.

In the experimental study, Hochstrasser and his co-workers[12] investigated the coherent excitation energy transfer between two identical chromophores in 9,9′-bifluorene and 2,2′-binaphthyl in different solvents at room temperature; the anisotropy decay of transient absorption in binaphthyl exhibited a damped oscillation corresponding to the excitation recurrence associated with the interaction energy (2β) of 41 cm^{-1} and the dephasing time (T_2') of 0.2 ps. Recently we reported a damped oscillation that appeared on the fluorescence anisotropy decay in an anthracene dimer, 2,15-dithia[3,3](1,5)anthracenophane (DTA, as shown in Fig. 1).[13] Although our experimental data of damped oscillation are quite impressive, as evidenced by the close agreement with the theoretical prediction, the contribution of the oscillating part is very small relative to the overall anisotropy signal. In order to observe the coherent dynamics more precisely, one must use a molecular system in which two chromophores are connected rigidly so that the dimeric conformation is fixed with a specific energy transfer interaction and a well-defined energy level structure. Subsequently, we reported a preliminary experiment on the coherent behaviors in the exciton motion for several anthracene dimers.[14]

We here report a comparative study on the coherent recurrence motion of exciton for different types of anthracene dimers in which two anthracene rings are connected closely. Figure 1 illustrates the structures of compounds concerned here. The present study will establish that the coherent recurrence motion of exciton between coupled chromophores will survive or outlast the dephasing process even in a room-temperature solution if one uses specially designed molecular systems of rigid dimeric conformation. In the present paper, first the theoretical background and formulation for the recurrence motions of exciton is presented in section 2. In sections 3 and 4, the oscillatory behaviors in fluorescence anisotropy decays are shown for various types of anthracene dimers, and the results of theoretical analyses are presented. In the last section, section 5, overall kinetic behaviors are discussed in relation to the phase relaxation time and the molecular structures.

1. Experimental

The picosecond fluorescence decay kinetics were measured with a time-correlated single-photon counting (TCPC) apparatus.[15] The femtosecond fluorescence decays were taken with a fluorescence up-conversion method composed of a femtosecond pulse laser and polarization anisotropy detection system.[16] The experimental setup is shown in Fig. 2.

The excitation light pulse source was the second harmonic of a Ti:Sappire laser (Spectra Physics Tsunami, 816 nm, 80 MHz)

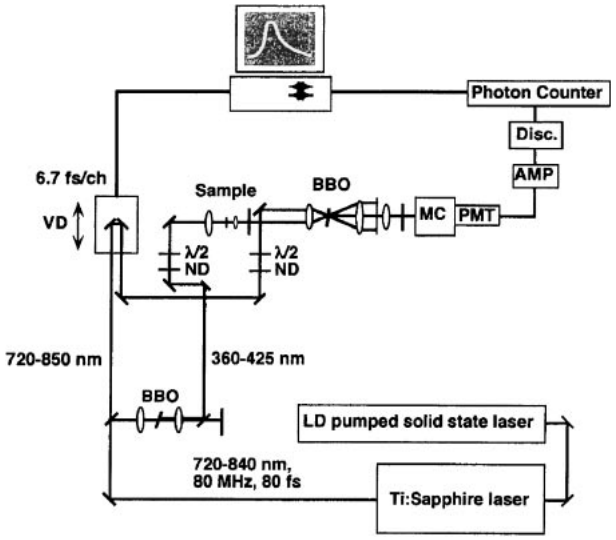

Fig. 2. Schematic diagram of experimental setup for fluorescence upconversion method. Disc., discriminator of photoelectron pulse; PMT, photomultiplier; MC, monochromator; ND, neutral density filter; VD, valuable optical delay line.

pumped with a diode-pumped solid state laser (Spectra Physics, Millenia X). The output laser pulse had a pulse width of 80 fs (FWHM), and a pulse energy of 16 nJ at 816 nm. Approximately half of the laser light was frequency doubled in a BBO crystal for excitation of the sample (0.5 nJ at 408 nm), and the remainder was used for the gating pulse. The gating pulse is passed through a variable delay line composed of a step-motor driven translation stage (Sigma STM-20X) which has the minimum displacement of 1.0 mm (corresponding to the delay time of 6.7 fs) under computer control. The fluorescence emission and the gating pulse were focused by a lens of 5.0-cm focal length into a BBO crystal of 0.5-mm thick. The wavelength of the up-conversion signal was adjusted by rotating the BBO crystal in a type-1 phase matching geometry. The wavelength of the detected signal, in practice, was approximately 290 nm, corresponding to a fluorescence wavelength of 450 nm. The sum frequency signal was filtered and frequency-selected by using a monochromator (JASCO CT-10) and a single-photon counting instrument equipped with a Hamamatsu R106UH photomultiplier.

The spectral width of the excitation laser pulse (the uncertainty-principle limited pulse) is estimated from the relation $\Delta\nu \cdot \Delta t \geq 0.44$ between the spectral width $\Delta\nu$ and the laser pulse width Δt. From the pulse width of the laser used in this study, $\Delta t =$ 70 fs, so the spectral width is $\Delta\nu$ (FWHM) $\geq$211 cm^{-1}. Since the magnitude of energy transfer interaction 2β for DTA is calculated to be 10–80 cm^{-1}, as shown in Section 5.1, the two eigenstates split by 2β may be excited coherently by using the present light source.

The two polarization components of fluorescence up-conversion signals, i.e., parallel ($I_\parallel$) and perpendicular ($I_\perp$) to the polarization plane of the excitation laser light, were measured alternately for the time-dependent fluorescence anisotropy. The data taken several times from alternate measurements were collected, and the anisotropy $r(t) = \{I_\parallel(t) - I_\perp(t)\}/\{I_\parallel(t) + 2I_\perp(t)\}$ were calculated as a function of time. The fluorescence decay curves and the anisotropy decay curves were measured, respectively, with a time-correlated single-photon timing apparatus for the ps time region and with a fluorescence up-conversion method for the fs time region.

All experiments were carried out at room temperature. The concentration of each sample solution was $\sim 10^{-5}$ M, and a sample cell 1-mm thick was used.

2. Theory of Recurrence Motion of Excitation

A Scheme of Exciton Interaction and Time-Evolution of Locally Excited States. The recurrence motion of excitation in a molecular system consisting of two identical chromophores can be formulated theoretically by the time-dependent perturbation theory. Figure 3 illustrates a scheme of the interchromophore interaction related to the recurrence motion of local excitation in a molecular dimer. Suppose an excited state is generated by the S_1 (^1L_a) $\leftarrow S_0$ transition of either half of the bichromophore. A singly excited state of this system is described as a product of the wavefunctions of the excited state of moiety a, ϕ_a', and the ground state of the other moiety b, ϕ_b, i.e., $\phi_1 = \phi_a'\phi_b$ (the prime stands for the excited state). Similarly the other excited state of the system is defined as $\phi_2 = \phi_a\phi_b'$. These two degenerate states ϕ_1 and ϕ_2, which are the eigenfunctions of the zeroth-order Hamiltonian H_0, can interact with each other through a Coulombic resonance interaction which can be approximated as a dipole–dipole interaction. From the first-order perturbation calculation, the resonance interaction creates two superposition states: $\psi_1 =$

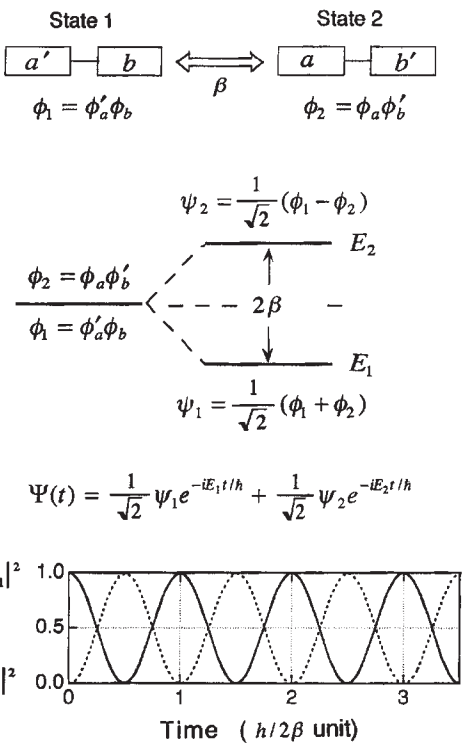

Fig. 3. Diagramatic illustration of the interchromophore interaction (β) in a dimer of a and b, and the creation of the two superposition states ϕ_1 and ϕ_2 split by 2β. In the expression $\phi_a\phi_b'$ or $\phi_a'\phi_b$, the prime stands for the excited singlet state of the chromophore. When the two states are excited coherently with an ultrashort pulse laser, the quantum state undergoes a time evolution. The recurrence motion of excitation is shown in the bottom.

$(1/\sqrt{2})(\phi_1 + \phi_2)$ and $\psi_2 = (1/\sqrt{2})(\phi_1 - \phi_2)$, which are the stationary states appearing in the static spectrum with a splitting of the interaction energy 2β. When the two superposition states are excited coherently by an ultrashort pulse laser of particular polarization, the quantum state is no longer a stationary state and undergoes a time evolution expressed as

$$\Psi(t) = \frac{1}{\sqrt{2}}\psi_1 e^{-iE_1 t/\hbar} + \frac{1}{\sqrt{2}}\psi_2 e^{-iE_2 t/\hbar}. \quad (1)$$

Taking the probability density of the quantum state in Eq. 1, we obtain

$$|\Psi(t)|^2 = (1/2)\psi_1^2 + (1/2)\psi_2^2 + \psi_1\psi_2 \cos[(E_1 - E_2)t/\hbar] \quad (2)$$

where the third term manifests a time evolution generated from interference between the two states ψ_1 and ψ_2. Rewriting Eq. 2 by using the original basis functions ϕ_1 and ϕ_2, we obtain the following equation:

$$|\Psi(q,t)|^2 = \cos^2(\beta t/\hbar)\phi_1^2 + \sin^2(\beta t/\hbar)\phi_2^2. \quad (3)$$

This alternative expression provides us with a more appropriate expression that an excitation localized on either half of a bichromophore moves back and forth between the two chromophores with a time period of $h/2\beta$. The oscillatory changes of the probability densities of ϕ_1 and ϕ_2 are illustrated in Fig. 3. The angular frequency of an oscillatory curve of the local excitation ϕ_1, for example, is related to the energy transfer interaction β. This oscillatory behavior can be observed in principle by detecting selectively the fluorescence component generated from either ϕ_1 or ϕ_2. Note that the relative orientations of the electronic transition dipole moments in the two chromophores are different. As described later, the actual measurement for each particular polarization component is performed by using the photoselection method.

One should note here that the theoretical scheme mentioned above is for a special case in which either half of two chromophores is initially excited. Actually there is a continuum of different initial conditions making different superpositions that are used in an average over the ensemble. Also noteworthy is the fact that such a recurrence could appear only in a short time (<1 ps) because the electronic dephasing process may be so fast that the macroscopic quantum coherence is lost rapidly in the condensed phase.

Rate Equation Including the Dephasing Process. Usually, molecules in solution undergo solute–solvent interactions that will change at each instant the electronic transition frequency and the energy transfer interaction. Such random and chaotic modification of the energy transfer interaction causes the reaction dynamics of an ensemble to change from a coherent to an incoherent process. In order to formulate the coherent reaction dynamics involving the dephasing process, the quantum mechanical treatment is performed on the basis of the density matrix. The time evolution of the density matrix elements ρ_{11} and ρ_{22}, i.e., populations of the states ϕ_1 and ϕ_2, respectively, can be expressed by the following differential equation which is derived from the optical Bloch equations:[17]

$$\Delta\ddot{n} + \left(\frac{1}{T_1} + \frac{2}{T_2}\right)\Delta\dot{n} + \left(4\beta^2 + \frac{2}{T_1 T_2}\right)\Delta n = 0. \quad (4)$$

Here Δn is the population difference $\Delta n = \rho_{11} - \rho_{22}$; β is the energy transfer interaction energy; and the phenomenological decay times T_1 for populations and T_2 for coherence are connected in a relation $1/T_2 = 1/(2T_1) + 1/T_2'$, where T_2' is the pure dephasing time (i.e., the decay of ρ_{12}). The differential equation of Eq. 4 can be solved for the three cases, depending on the ratio of the interaction energy 2β to the energy width of the pure dephasing process (T_2'). In the underdamped condition $2\beta T_2' > 1$, the following solution is obtained:[18–20]

$$\Delta n(t) = \frac{\Delta n(0)}{\cos\delta} e^{-\gamma t}\cos(\omega_{\mathrm{osc}} t + \delta) \quad (5)$$

where

$$\gamma = \frac{1}{T_1} + \frac{1}{T_2'}, \quad \omega_{\mathrm{osc}} = \sqrt{4\beta^2 - \left(\frac{1}{T_2'}\right)^2}$$

and

$$\tan\delta = -\frac{1}{\omega_{\mathrm{osc}}}\left(\frac{1}{T_1} + \frac{1}{T_2'}\right). \quad (6)$$

A sum of populations $S = \rho_{11} + \rho_{22}$ is derived also from Bloch equations as follows:

$$S(t) = e^{-\left(\frac{1}{T_1}\right)t} S(0). \quad (7)$$

Equation 5 shows that the population difference $\rho_{11} - \rho_{22}$ oscillates at an angular frequency ω_{osc}, but the oscillation does not continue indefinitely and is damped with a rate $1/T_1 + 1/T_2'$. Equation 7 shows that the sum of populations $\rho_{11} + \rho_{22}$ decays exponentially with a rate $1/T_1$, which corresponds to the ordinary fluorescence decay obtained by the magic angle excitation.

Expression for the Fluorescence Anisotropy Decay. In an experiment for observing a recurrence motion of excitation through the fluorescence anisotropy decay, we need to correlate the propagators for the density matrix elements ρ_{11}, ρ_{12}, ρ_{21}, and ρ_{22} with the respective polarization components of fluorescence intensity. The magnitude of the density matrix element depends not only on the strength of the transition dipole moment but also on the projection of the pump pulse polarization in the laboratory frame onto the transition dipole moment vector. The polarized fluorescence intensity $I(t)$ is obtained after calculation of the stochastic averages of the correlation functions for an isotropic medium as follows:[18–20]

$$I(t) = 2\langle l_x l_y p_x p_y\rangle e^{-\gamma t} + \langle l_x^2 p_x^2\rangle[1 + f(t)] + \langle l_x^2 p_y^2\rangle[1 - f(t)] \quad (8)$$

where $f(t)$ is the term of the damped oscillation in Eq. 5, i.e.,

$$f(t) = e^{-\gamma t}\cos(\omega_{\mathrm{osc}} t + \delta) \quad (9)$$

l_{i}, m_{i}, and n_{i} are the direction cosines of the field polarization vector onto the molecular polarization dipole i, and p_{i} is that for the probe emission polarization. We consider first the case where the electronic transition dipole moments coincide between the excitation absorption and the probe fluorescence. If p_{i} is chosen parallel to the pump polarization, we obtain $I_{\parallel}(t)$ with the substitutions $p_x = l_x$, $p_y = l_y$; if it is perpendicular, we obtain $I_{\perp}(t)$ with the substitutions $p_x = m_x$, $p_{\mathrm{y}} = m_{\mathrm{y}}$. After calculating the average of the correlation function, the anisotropy is expressed as;

$$r(t) = \frac{I_{\parallel}(t) - I_{\perp}(t)}{I_{\parallel}(t) + 2I_{\perp}(t)} = \frac{1}{10}[1 + 3f(t) + 3e^{-\gamma t}] \qquad (10)$$

where $\gamma = 2/T_2'$. It is worth noting that $I_{\parallel}(t) + 2I_{\perp}(t)$ is a constant value 10/15, suggesting that the isotropic decay shows no oscillation. In the case of a dimer as in the present case, the equation for $r(t)$ is expressed as:[18]

$$r(t) = \frac{r(t) + \frac{1}{10}[3 + e^{-\gamma t} - 3f(t)]\cos^2\theta}{1 + e^{-\gamma t}\cos^2\theta}$$
$$= \frac{0.1}{1 + e^{-\gamma t}\cos^2\theta}[(1 + 3\cos^2\theta) + 3f(t)(1 - \cos^2\theta) + (3 + \cos^2\theta)e^{-\gamma t}] \qquad (11)$$

where θ is the angle between the transition dipole moments of the two chromophores. Equation 11 means that the fluorescence anisotropy depends on the angle between the transition dipole moments of the two chromophores; the second term generates the oscillation with its amplitude depending on θ; when $\theta = \pi/2$ the amplitude is largest, but when $\theta = 0$ the oscillation is not observed. In the case of DTA, for example, θ is near 90° and $\cos\theta \approx 0$, so Eq. 10 is the proper one to be used for analyzing the present experiments. Equations 10 and 11 suggest that the excitation population in either half of bichromophore undergoes an oscillation with an angular frequency ω_{osc}, but the oscillation is damped exponentially with a time constant determined by the phase relaxation time. In the present case, γ is approximated to be $1/T_1 + 1/T_2' \approx 1/T_2'$, since $1/T_1 \ll 1/T_2'$ (T_1 = 3–7 ns in the anthracene dimers studied).

Therefore, an analysis of the oscillatory pattern based on Eq. 10 or 11 provides us with information on the interchromophore interaction energy and the electronic dephasing time.

3. Anthracene Dimers[14]

Two anthracene dimers (Fig. 1) were synthesized: 1,2-bis(anthracen-9-yl)benzene (*o*-DAB) and 3,5-bis(anthracen-2-yl)-*t*-butylbenzene (*m*-DAB).[14] The X-ray crystallography for *o*-DAB showed a dihedral angle 66.2° between the two anthracene rings with the center-to-center distance $r_0 = 5.13$ Å. For *m*-DAB, the dihedral angle in the most stable conformation was estimated to be ca. 60° and $r_0 = 10.2$ Å was found from MO calculations. All the experiments were carried out for toluene and THF solutions with a concentration of ca. 10^{-5} M at room temperature (296 K).

Absorption and Fluorescence Spectra. The absorption and fluorescence spectra of *m*-DAB and *o*-DAB in toluene solution are shown in Fig. 4, together with those of the anthracene monomer. The absorption spectra of the dimers for the $S_1 \leftarrow S_0$ transition are approximately similar to that of anthracene monomer with several vibronic bands, but red-shifted by 10 nm. The spectral profiles are somewhat diffuse relative to that of the monomer; the bandwidth of the 0–0 band (FWHM) is 880 cm^{-1} in *m*-DAB and 1050 cm^{-1} in *o*-DAB, while that of the monomer is 496 cm^{-1}. Such band broadening is caused predominantly by an inhomogeneous broadening due to conformation distribution of the dimers in solution, in addition to a spectral band overlap with a nearby vibronic band due to a ν_{12} (A_{1g}) vibrational mode of anthracene which appears as a shoulder in the monomer spectrum. The fluorescence spectra of the dimers show a mirror image with the absorption spectra, and diffuse similarly to the absorption. In the experiment for the fluorescence decay kinetics, the dimers were excited at 390 nm, i.e., the 0–0 band of $S_1 \leftarrow S_0$ (L_a) absorption, with a pulsed laser of pulse width 80 fs and spectral width $\Delta\nu = 190$ cm^{-1}.

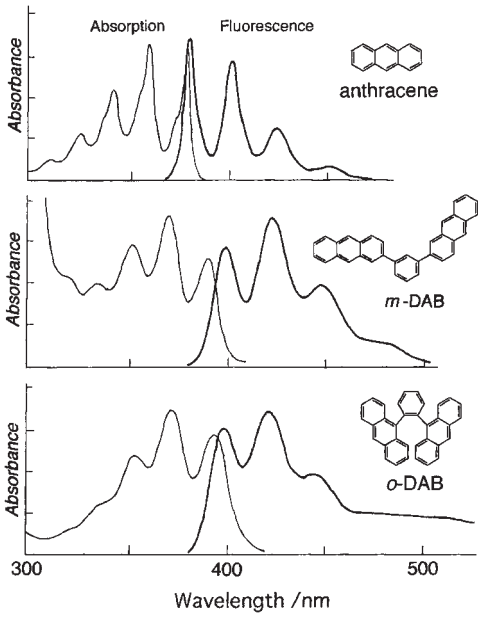

Fig. 4. Absorption (left) and fluorescence (right) spectra of anthracene dimers in toluene solution.

Fluorescence Decays and Fluorescence Anisotropy Decays. The two dimers, *m*-DAB and *o*-DAB in toluene, exhibit the fluorescence decay curves of single exponential form in the ps time region with the lifetime of 6.3 ns in *m*-DAB and 7.5 ns in *o*-DAB. The decay curve of *m*-DAB as an example is shown in Fig. 5a. These τ_F values are close to the values of anthracene monomer ($\tau_F = 5.24$ ns), suggesting that the excited-states population of the dimers decays with the lifetime of anthracene itself. The fluorescence anisotropy decays in ps time region (Fig. 5b) were also single exponential with the decay constants of 87 ps for *m*-DAB and 75 ps for *o*-DAB in toluene. These values can be considered reasonably to be time constants of the rotational diffusion of a whole molecule in fluid solution. The decay constants of fluorescence decays and fluorescence anisotropy decays are summarized in Table 1. The phenomena that we are interested in here take place on a time scale much shorter than that of the rotational diffusion of a molecule. Therefore the rotational diffusion effects can thus safely be ignored for the present analysis.

The fluorescence anisotropy decays $r(t)$ in the fs time region are shown in Figs. 6–8 for *m*-DAB and *o*-DAB together with the fluorescence decay obtained by the magic angle excitation. In every case, the ordinary fluorescence decay (excited-state population decay) $I_F(t)$ shows a instantaneous spike at the same time region as the excitation laser pulse, followed by a slow (seemingly flat) decay. The initial sharp pulse is recognized as arising from scattering of the excitation laser pulse, and the slow decay corresponds to the excited-state population decay that appears in the picosecond time domain. On the oth-

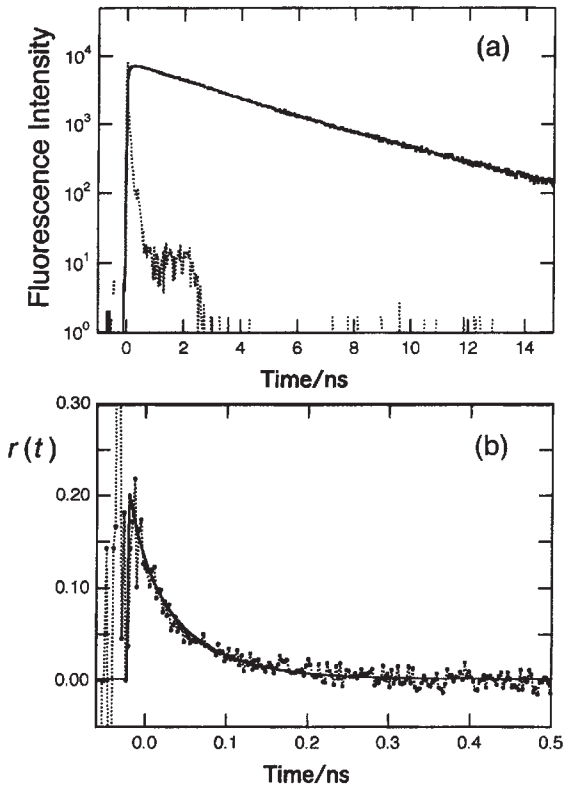

Fig. 5. Fluorescence decay (a) and fluorescence anisotropy decay curve (b) in picosecond time domain for *m*-DAB in toluene, measured with the TCPC apparatus. The wavelength of excitation is 310 nm, and the monitoring wavelengths are 430 and 500 nm.

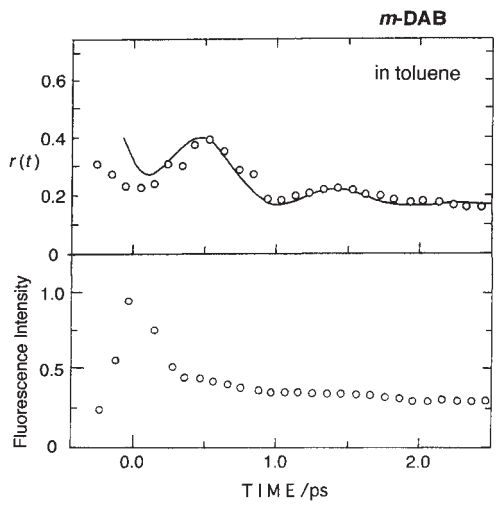

Fig. 6. Fluorescence anisotropy $r(t)$ (upper) and fluorescence decay (lower) curves in femtosecond time domain for *m*-DAB in toluene. The center wavelength of excitation laser light is 390 nm, and the monitoring wavelength is 427 nm. The solid line in $r(t)$ curve is the theoretical best fit curve.

er hand, the $r(t)$ curves in 0–2 ps time region exhibit distinct oscillation, followed by slow decays due to the rotational diffusion ($\tau_{rot} = 50$–90 ps). The time periods of oscillation are

Table 1. Decay Constants of Fluorescence (τ_F) and Fluorescence Anisotropy (τ_r) in Anthracene Dimers in Solution

Molecules	*m*-DAB		*o*-DAB	DTA
Solvents	THF	Toluene	Toluene	THF
τ_F/ns	5.2	6.3	7.5	0.063[a)] 3.2[b)]
τ_r/ps	50	87	75	45

a) Monitored at 430 nm. b) Monitored at 500 nm.

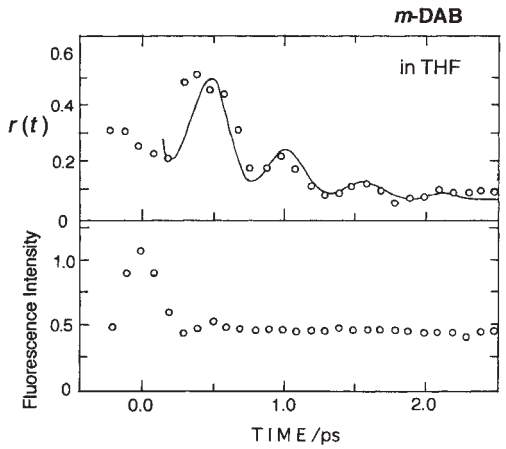

Fig. 7. Fluorescence anisotropy $r(t)$ (upper) and fluorescence decay (lower) curves in femtosecond time domain for *m*-DAB in THF. The center wavelength of excitation laser light is 390 nm, and the monitoring wavelength is 427 nm. The solid line in $r(t)$ curve is the theoretical best fit curve.

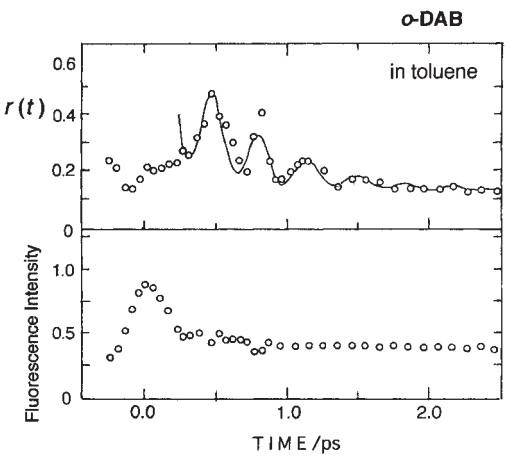

Fig. 8. Fluorescence anisotropy $r(t)$ (upper) and fluorescence decay (lower) curves in femtosecond time domain for *o*-DAB in toluene. The center wavelength of excitation laser light is 390 nm, and the monitoring wavelength is 427 nm. The solid line in $r(t)$ curve is the theoretical best fit curve.

0.34 ps in *o*-DAB and 0.91 ps in *m*-DAB in toluene, and the damping time constants γ are 1.0 ps in *o*-DAB and 0.73 ps in *m*-DAB. It is seen that the oscillatory behavior depends on the solvent: the time period of oscillation in *m*-DAB is shorter in THF (0.55 ps) than in toluene (0.91 ps).

Table 2. Characteristics of Coherent Energy Transfer Dynamics of Bichromophores in Solution at 296 K

Molecules	Solvents	T_{osc} / ps	ω_{osc} / 10^{12} rad·s^{-1}	T_2' / cm^{-1}	$2\beta_{exptl}$ / cm^{-1}	$2\beta T_2'$
m-DAB[a]	Toluene	0.91	6.9	0.73	37.4	5.1
	THF	0.55	11.4	0.78	61.0	9.0
o-DAB[a]	Toluene	0.34	18.5	1.02	98.2	18.9
DTA[b]	THF	1.0	6.3	1.2	33.6	7.6
Binaphthyl[c]	CCl_4	1.2	2.2	0.18	39.7	1.4

a) Present work. b) From Ref. 13. c) From Ref. 12. All the values are with an accuracy of about ±10%.

Table 3. Geometrical Parameters of Bichromophore Molecules in Solution

Molecules	R_0 / Å	θ_{12}[d] / degree	θ_1 / degree	θ_2 / degree	κ	$2\beta_{calc}$[e] / cm^{-1}
m-DAB[a]	10.2	60°	41°	79°	0.93	11.2
o-DAB[b]	5.13	66°	58°	58°	1.1	81.2
DTA[c]	3.41	81°	90°	90°	0.16	13.8

a) MO calculation by MOPAC. b) From X-ray crystallography. c) From X-ray crystallography. d) Calculated from the direction of the transition moment of constituent chromophore which were calculated from MO calculation by MOPAC. e) The dipole–dipole interaction energy calculated by using the geometrical parameters listed in this table and Eq. 13.

The oscillation patterns in anisotropy decays were analyzed with the theoretical equation (Eq. 11). From the observed $r(t)$ curve, the tentative values for the oscillation frequency (ω_{osc}) and the dephasing time (T_2') were evaluated. Using these values and a plausible value for θ, we fit the theoretical curves of Eq. 11 to the respective experimental curves by varying the δ value until the best fit curve was obtained. In these processes, the tentative parameter values were refined to obtain much more reasonable fitting. It is seen in Figs. 6–8 that the respective experimental curves are fitted to the theoretical curves (solid lines). Then using the values of ω_{osc} and T_2' thus obtained, we evaluated the interaction energy β from Eq. 6. The parameter values thus obtained are summarized in Table 2.

One striking feature of the results is that the interaction energy is two times larger in *o*-DAB ($2\beta = 98.2$ cm^{-1}) than in *m*-DAB ($2\beta = 37.4$ cm^{-1}). This difference is consistent with an expectation deduced from molecular structures (Fig. 1) and geometrical parameters (Table 3) for the two dimers; for an example, the interchromophore distance R_0 in *o*-DAB is one half of that in *m*-DAB; such a difference may result in a large difference in the interaction energy. In the Discussion section, we will discuss the origin of the interaction energies by reference to the values calculated on the basis of the Coulombic dipole–dipole interaction. Also noteworthy is that the dephasing time T_2' in *o*-DAB is longer than *m*-DAB. It appears that the pure dephasing time is correlated to the rotational degree of freedom of partial moieties. In *m*-DAB, the two anthracene rings can rotate around a single bond, whereas in *o*-DAB the librational motion of anthracene rings is suppressed by steric hindrance.

4. Dithiaanthracenophane (DTA)[13]

Similar undulating behavior to that as seen in DAB's was observed in 2,15-dithia[3,3](1,5)anthracenophane (hereafter referred to as DTA)[13,21] that has a pair of identical chromophores stacked rigidly. The molecular structure determined from X-ray crystallography is shown in Fig. 9. Two anthracene rings are connected through two thioethers at α positions almost parallel (dihedral angle 5.0°) with an interplanar distance of 3.41 Å and one of the rings is rotated by 88.5° around the center of the anthracene ring.[22] Therefore, DTA is suitable for examining the coherent dynamics of excitation transfer, since the spatial arrangement of two chromophores is rigid and gives a confined conformation of dimeric structure even in fluid solution. The nearly orthogonal orientation of the two anthracene rings, and therefore the orthogonal orientation of their transition dipole moment vectors, enable us to detect selectively the emission from the local excitation on ether half of bichromophore by using the photoselection method.

Absorption and Fluorescence Spectra. Figure 10 shows absorption and fluorescence spectra of DTA in THF. The absorption spectrum of DTA is similar to the anthracene spectrum with several vibrational bands. The stationary fluorescence spectrum in THF exhibits only a diffuse and broad band centered at 469 nm (curve 2 in Fig. 10), which is obviously different from the mirror image of the absorption band profile. Previously, we examined the picosecond time-resolved fluorescence spectra (see Fig. 2 of Ref. 22) in relation to the intramolecular excimer formation in DTA.[22] The fluorescence spectrum in a short time region (0–25 ps) exhibits a well-defined, structured spectrum, as shown in Fig. 10 (curve 1), with a mirror image of the absorption spectrum, while after 50 ps it changes into a broad and diffuse one centered at 469 nm which is identical to the stationary fluorescence spectrum (curve 2 in Fig. 10). From analyses of the fluorescence rise and decay curves as well as the time-resolved spectra, we assigned the structured band (0–25 ps) to a monomer fluorescence and the broad red-shifted band (after 50 ps) to an excimer fluores-

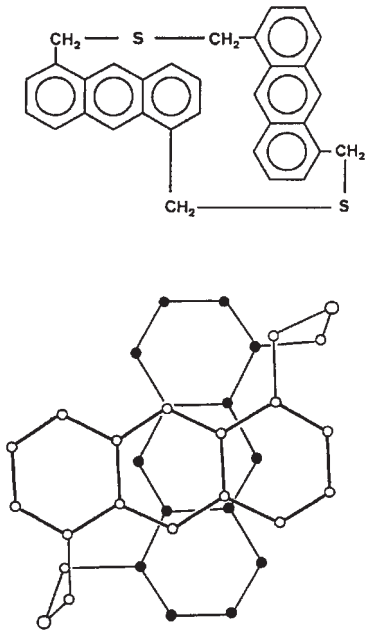

Fig. 9. (a) Molecular formula of dithiaanthracenophane (DTA), and (b) a view of DTA on least-squares plane defined with an anthracene ring determined from X-ray analysis.

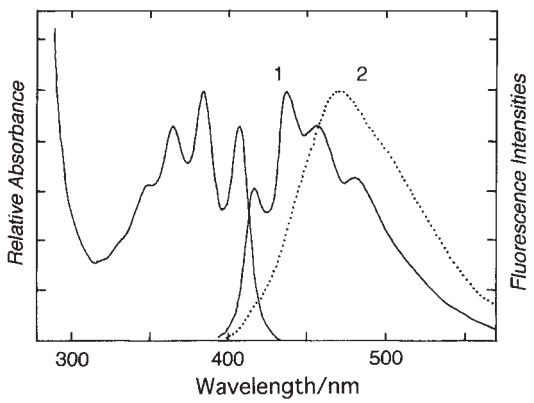

Fig. 10. Absorption (left) and fluorescence (right) spectra of DTA in THF solution. Curve 1 is the time-resolved fluorescence spectrum in 0–25 ps taken from Fig. 2 in Ref. 22, and curve 2 is the stationary fluorescence spectrum.

cence. Since we are concerned here with the time domain shorter than 5 ps, we are therefore able to neglect the excimer process and to confine our discussion to the excited-state dynamics under the stronger energy-transfer interaction.

Fluorescence Decays and Fluorescence Anisotropy Decays in ps Time Domain. Figure 11 shows the picosecond fluorescence decay curves measured with a time-correlated, single-photon counting (TCPC) apparatus. The decay curve depends on the monitoring wavelength; the decay curve monitored at 430 nm is biexponential with the lifetimes of $\tau_F = 63$ ps and 3.2 ns, while at 500 nm it is almost single exponential with $\tau_F = 3.2$ ns. Note that the time-resolved fluorescence spectra of DTA, as mentioned above, show the spectrum of the anthracene monomer in a time region of 0–25 ps. Then it

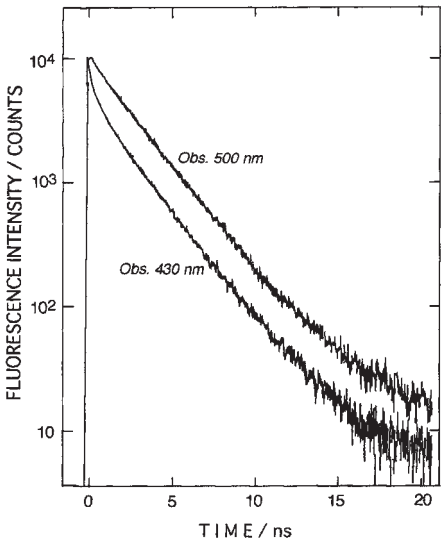

Fig. 11. Fluorescence decay curves of DTA in THF, obtained with the picosecond TCPC apparatus. The wavelength of excitation is 310 nm, and the monitoring wavelengths are 430 and 500 nm.

follows that the 63-ps lifetime corresponds to the time constant of the excimer formation between the excited and unexcited chromophores, and the lifetime of 3.2 ns corresponds to the deactivation of the excimer state to the ground state of monomer. The $r(t)$ curve in the picosecond time domain (Fig. 12b), which was measured with the TCPC system at 450 nm, shows a rather slow decay which can be well fitted to a single exponential decay with 45-ps time constant. The molecular process which randomizes the fluorescence anisotropy in the picosecond time region is recognized to be due to the rotational diffusion. It will be reasonable from comparison to the corresponding values of DAB ($\tau_r = 50$–90 ps) and binaphthyl ($\tau_r = 35$ ps).[12] Then it follows that the excited-state population decay kinetics and the rotational diffusion kinetics both occur on a much slower time scale than the intramolecular energy transfer concerned here, and the internal angular jump of excitation could be viewed as occurring in a relatively fixed dimer orientation. The decay constants obtained from the fluorescence decay and anisotropy decay are summarized in Table 1.

Fluorescence Decays and Fluorescence Anisotropy Decays in fs Time Domain. Figure 12a shows the fluorescence anisotropy decays in a femtosecond time region for DTA in THF solution at 296 K. In this measurement, DTA was excited around the 0–0 band of ^1L_a absorption transition with a laser pulse with a center wavelength of 408 nm (see Fig. 10). The $r(t)$ curve in femtosecond time domain, which was obtained with fluorescence up-conversion technique monitored at 450 nm, shows that an oscillatory change is superimposed on the slow (flat) decay in 0–4 ps, and that the anisotropy starts from a certain negative value as is seen around $t = 0$. Monitoring the fluorescence at 500 nm, however, gives only a very weak oscillation on the decay curve (see Fig. 4 in Ref. 13). When the excitation is performed at a longer wavelength band edge of the 0–0 band at 415 nm (see Fig. 4 in Ref. 13), there appears no oscillatory pattern, and the decay curve can be fitted with a single exponential decay.

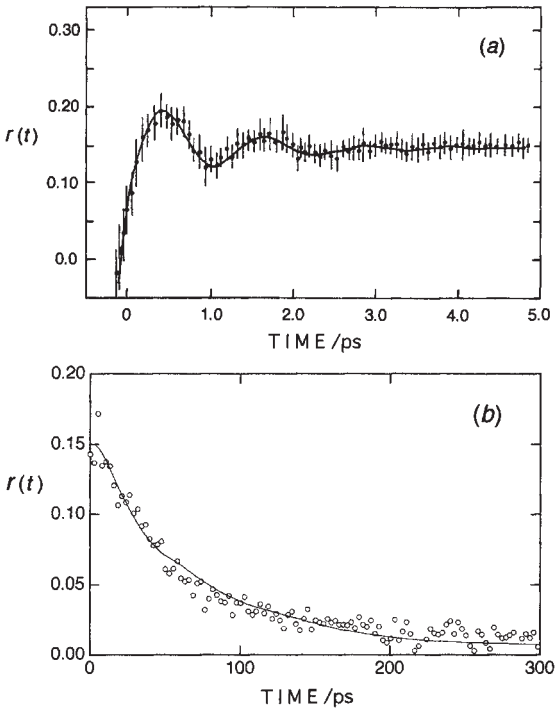

Fig. 12. (a) Femtosecond fluorescence anisotropy decay of DTA in THF, measured with the fluorescence up-conversion apparatus. The excitation wavelength is 408 nm, and the monitoring wavelength is 450 nm. The standard deviation in four sets of measurements is shown in vertical lines. (b) Picosecond fluorescence anisotropy decay measured with the TCPC apparatus. The excitation and monitoring wavelengths are the same as those in (a). The solid line is the best-fitted curve calculated by using a single exponential form with 45-ps time constant.

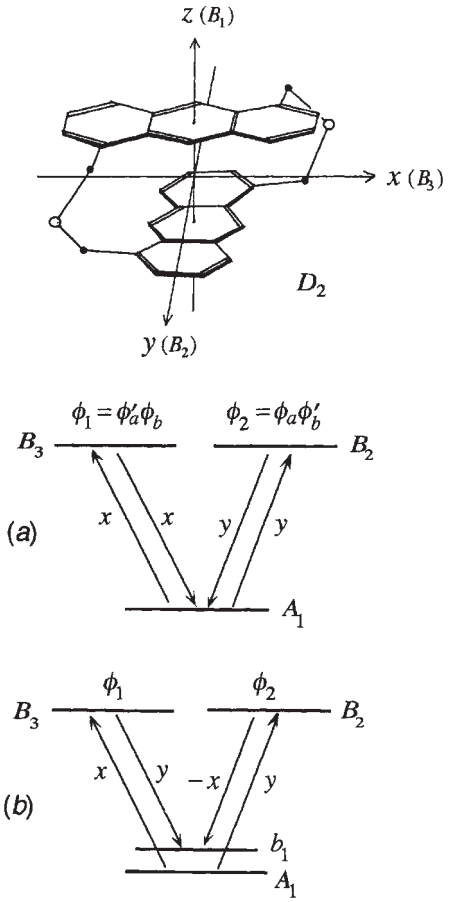

Fig. 13. Energy level scheme with symmetries of states and directions and signs of transition dipole moments in the frame of a molecule with D_2 symmetry. The x- and y-axes are taken to be orthogonal to the D_2 rotation axis (z-axis). (a) The usual case for fluorescence. (b) An alternative case that involves out-of-plane (z-polarized) transition due to involvement of a b_1 vibrational state in the final electronic state.

Analysis of Oscillatory Anisotropy Decays. The theoretical equation (Eq. 10) for the fluorescence anisotropy decay holds for the usual case where the electronic transition dipole moments for the excitation (absorption) and the probe (fluorescence) processes coincide, as shown in Fig. 13a. Equation 10 predicts that the anisotropy at very short time before dephasing has a value of $r = 0.7$; then this value decreases to $r = 0.4$ due to electronic dephasing. When the two degenerate states ϕ_1 and ϕ_2 are completely dephased by the incoherent coupling, the anisotropy attains a value of $r = 0.1$. Contrary to such a theoretical prediction for the usual case, however, the experimental anisotropy decay $r(t)$ shown in Fig. 12a starts with negative value at $t = 0$ and then it converges on $r(t) = +0.15$ after damping oscillation. We assume, therefore, that another fluorescence component whose anisotropy is negative at $t = 0$ is involved in the probed fluorescence. In the case that the final state of fluorescence transition is a vibrational state of a nontotally symmetric vibration, the fluorescence transition moment could be perpendicular to the absorption transition moment. This view might be supported by the experimental condition that the anisotropy decay is monitored at 450 nm, i.e., a spectral region corresponding to a vibrational level of 1800 cm^{-1} (one quantum of b_1 vibrational mode, see below) above the 0–0 transition energy.

For the case that the fluorescence transition dipole is perpendicular to the absorption dipole through a coupling to a non-totally symmetric vibration in the final state, as shown in Fig. 13b, the expression for $I_{\parallel}(t)$ is obtained from Eq. 8 with the substitutions $p_x = l_y$, $p_y = -l_x$ as $(2/15)\{2 - f(t) - e^{-\gamma t}\}$, and that for $I_{\perp}(t)$ is obtained with the substitutions $p_x = m_y$, $p_y = -m_x$ as $(1/15)\{3 + f(t) + e^{-\gamma t}\}$. As a result, we obtain the anisotropy decay as

$$r(t) = \frac{1}{10}\{1 - 3f(t) - 3e^{-\gamma t}\}. \tag{12}$$

One should note that $I_{\parallel}(t) + 2I_{\perp}(t)$ is a constant value 10/15, as in the usual case mentioned before. Equation 12 shows that the value of anisotropy is $r = -0.5$ at $t = 0$, then $r = -0.2$ after dephasing and $r = 0.1$ after population equalization. We assume that the fluorescence monitored at 450 nm is a superposition of the two vibronic transitions: one is coupled to a totally symmetric vibration and the other is coupled to a nontotally b_1 vibration. The resultant time-dependent anisotropy is a sum of the two anisotropy curves of Eqs. 10 and 12. The best fit curve was obtained with the ratio 1:0.35 of the amplitude of the former function in Eq. 10 to that of the latter function in

Eq. 12. The solid line in Fig. 12a is the best fit to the experimental curve. We obtain $\omega_{osc} = (6.3 \pm 0.2) \times 10^{12}$ rad·s^{-1} and $T_2' = 1.2 \pm 0.1$ ps, leading to the resonance energy transfer interaction $2\beta = 33.6$ cm^{-1}.

Note that DTA has D_2 symmetry and the state ϕ_1 and ϕ_2, belong to B_2 and B_3 symmetry classes, respectively. The vibrational state which gives the transition dipoles perpendicular to the absorption transition should have b_1 symmetry. From the MO calculation using the PM3 method as parametrized within the MOPAC 93.0,[23] DTA has several normal vibrations belonging b_1 symmetry in a range of $\sim$1800 cm^{-1}. Therefore, the probed fluorescence is due to the transition from a level of ^1L_a (0–0) to a vibronic level of one vibrational quantum of b_1 symmetry mode.

5. Discussion

The present experimental results revealed the oscillatory behaviors for several types of anthracene dimers on the fluorescence anisotropy decays in the very short time region (<3 ps). In this section, we will discuss the origins of such oscillations in view of the quantum beat due to an quantum coherence effect, i.e., the coherent recurrence motion of an exciton wavepacket. The magnitude of the energy transfer interaction energy derived from the beat frequency is compared to those from the theoretical calculation. The electronic dephasing time derived from the analyses will be discussed in comparison with the previous results regarding binaphthyl and bifluorene reported by Hochstrasser's group.[12]

5.1 Energy Transfer Interaction—Estimation Based on the Dipole–Dipole Interaction between Two Chromophores. We analyzed the oscillation patterns of fluorescence anisotropy decays according to the theoretical scheme of exciton interaction between two chromophores, and derived a magnitude of energy transfer interaction ranging from 50 to 100 cm^{-1} depending on the dimer structure. It must be crucial to ensure that these interaction energies are reasonable from viewpoints of the exciton interaction, i.e., the dipole–dipole resonance interaction or some other interaction between two coupled anthracene rings. Direct information on the interchromophore interaction energy is given in principle from the absorption spectrum of a dimer in supersonic molecular beam; the band splitting in a particular vibronic band, the 0–0 band for example, may give directly the exciton interaction energy 2β (see Fig. 3). In the absorption spectrum in solution, this sort of interaction may result in band broadening. In the present cases, the full-width of half maximum (FWHM) of the 0–0 band is 496 cm^{-1} in anthracene monomer, 880 cm^{-1} in *m*-DAB, 1056 cm^{-1} in *o*-DAB, and 850 cm^{-1} in DTA. The band broadenings on going from the monomer to dimers are recognized as due predominantly to the structural distribution of dimer conformation (inhomogeneous broadening) because the spectrum taken at 77 K for rigid glass gives a narrow spectrum similar to those of the anthracene monomer. Furthermore, the spectral overlap with the ν_{12} vibronic band nearby the 0–0 band makes it difficult to deduce the band splitting due to the interchromophore interaction. Then we calculated the interaction energy due to the dipole–dipole resonance interaction scheme for various types of anthracene dimers.

The dipole–dipole interaction energy is expressed as

$$\beta = \frac{1}{4\pi\varepsilon_0\varepsilon}\frac{e^2|\mathbf{M}_{00}|^2}{R^3}\kappa \tag{13}$$

where e is the elementary charge, $\mathbf{M}_{00}$ is the transition dipole moment for the 0–0 vibronic transition, R is the distance between the centers of chromophores, and ε_0 and ε are the permittivities of free space and of the solvent, respectively. The orientation factor κ is defined as $\kappa = \cos\theta_{12} - 3\cos\theta_{1R}\cos\theta_{2R}$, where θ_{12} is the angle between the transition dipole moments for the two chromophores, θ_{1R} is the angle between the transition moment of one chromophore and the distance vector $\mathbf{R}$, and θ_{2R} is the angle for the other chromophore. In the present cases where the exciton splitting for 0–0 band is important, the electronic transition dipole moment $\mathbf{M}_{00}$ is taken into consideration instead of the overall transition dipole moment for $S_1 \leftarrow S_0$, $\mathbf{M}$.

The values of $\mathbf{M}_{00}$ can be estimated from the experimental data and literature value for the overall transition dipole moment for $S_1 \leftarrow S_0$, i.e., $\mathbf{M} = 0.601 \times 10^{-10}$ m (estimated from the oscillator strength $f = 0.11$[24]). The relationship between $\mathbf{M}_{00}$ and $\mathbf{M}$ is expressed through the Franck–Condon factor as follows:

$$\begin{aligned}|\mathbf{M}_{00}|^2 &= |\mathbf{M}|^2 \times |\langle\Lambda_{10}(Q)|\Lambda_{00}(Q)\rangle|^2 \\ &= \left|\langle\Psi_1(q,Q)\left|\sum_j r_j\right|\Psi_0(q,Q)\rangle\right|^2 \\ &\quad \times |\langle\Lambda_{10}(Q)|\Lambda_{00}(Q)\rangle|^2\end{aligned} \tag{14}$$

where $\Psi_i(q,Q)$ is the i th electronic state wavefunction when the nuclei are at Q and the electrons are at q, Λ_{ik} is the k th vibrational wavefunction in the electronic state Ψ_i, and r_j is the spatial coordinates of the j th electron. The second term of Eq. 14 is the vibrational overlap integral (Franck–Condon factor) for the 0–0 transition of $S_1 \leftarrow S_0$ (^1L_a). If the overall transition dipole moment for $S_1 \leftarrow S_0$ is considered, a summation is taken over all the vibronic transitions involved in the $S_1 \leftarrow S_0$ transition, and it gives unity: $\sum_k |\langle\Lambda_{1k}(Q)|\Lambda_{00}(Q)\rangle|^2 = 1$. The magnitude of the Franck–Condon factor for each of the vibronic transitions can be estimated from the relative absorption intensities of respective vibronic bands; in the present case of anthracene, the integrated band intensities for each vibronic band were obtained for toluene solution as: 0.313 for 0–0 band, 0.258 for 1–0 band, 0.230 for 2–0 band, and 0.080 for 3–0 band (the total amount of these primary bands is 0.981). Here we are concerned with the exciton splitting at 0–0 absorption band; then the exciton interaction energy (Eq. 13) is calculated by using $|\mathbf{M}_{00}|$, i.e., a value of 0.313 times the overall transition dipole moment.

The interchromophore distances and the orientational factors used in the calculation are listed in Table 3. For *o*-DAB, the geometrical parameters are taken from the X-ray crystallography results, while for *m*-DAB these are estimated from the most stable conformation obtained from the MO calculation with the CNDO/S3 by MOPAC 93.0.[23] In the case of DTA, geometric parameters are taken from the X-ray crystallography results; the two planar anthracene rings are stacked in parallel to each other with the interplanar distance of $R_0 =$ 3.41 Å and the angle between the respective short axes of

two anthracene rings of 88.5°. For the angle between the electronic transition moments θ_{12}, the value taken from the MO calculation was used. The electronic transition dipole moment must be displaced from that of anthracene monomer (the short axis for ^1L_a) because of α-substitution in DTA. From the MO calculation with the CNDO/S3 by MOPAC 93.0[23] for anthracene-1,5-diylbis(methanethiol), the angle between the transition moment and the short axis of anthracene ring is estimated to be 4.5°, and therefore the θ_{12} value is 81.0°. This value was used for θ_{12} in DTA.

By using these values, we calculated the interaction energies 2β for *m*- and *o*-DAB and DTA. The results are listed in Table 3. The calculated values $2\beta_{calc}$ in all the cases are somewhat smaller than the experimental ones $2\beta_{exptl}$, particularly in *m*-DAB and DTA. This difference may be regarded as due to some inadequacy of the point dipole approximation and/or some contribution from the interchromophore interactions other than the dipole–dipole interaction, e.g., electron exchange interaction. Particularly, it is expected that the close parallel packing in DTA ($R_0 = 3.4$ Å) can induce the intramolecular charge resonance interaction, and will enhance the interchromophore interaction. As a consequence, the interaction energies derived from the experimental oscillatory behaviors are interpreted reasonably in terms of the interaction energy arising from the dipole–dipole interaction and/or the charge resonance interaction. Then it follows that the oscillations on fluorescence anisotropy decay are accounted for as due to the electronic coherence, and originate from the coherent recurrence motion of an exciton. This view is evidenced from our recent study of the phase-locked, double-pulse excitation method.[25]

5.2 Dephasing Times. The electronic coherence observed in the present study is an interference effect between two time-evolutionary quantum states. The necessary condition for exposing this effect as a macroscopic quantum coherence is that the phase of the time evolution of quantum states is the same among the molecular systems in an ensemble. Usually molecules in solution undergo solute–solvent interaction at each instant, so that individual molecular systems in an ensemble undergo random and chaotic fluctuation of the energy levels and the energy transfer interactions. This may randomize the quantum phase of the time-evolutionary quantum state in an ensemble, and cause the energy transfer to change from a coherent to an incoherent process. In the optical Bloch equation expressed in Eq. 4, this randomizing process is taken into account as a relaxation process with a time constant defined as T_2'. This pure dephasing time T_2' can be determined from the damping time constant of oscillatory behavior which appears on fluorescence anisotropy decays. In other words, the measurement of the quantum coherence gives direct information on the electronic dephasing time.

Correlation between the Dephasing Time and the Librational Motion of Chromophores: The dephasing times obtained in this study for anthracene dimers are summarized in Table 2 together with the data for binaphthyl. It can be seen that the T_2' value is longer in DTA and *o*-DAB relative to those in *m*-DAB and binaphthyl irrespective of the magnitude of interaction energy. The two cases of DTA and *o*-DAB are characterized by rigid dimer conformations (see Fig. 1); in DTA, the two anthracene rings are connected through two thioether chains, and in *o*-DAB, the two anthracene rings cannot rotate because of the steric hindrance. The dimer structures are almost fixed in a very close arrangement. On the other hand, the other two cases of *m*-DAB and binaphthyl have flexible conformations due to twisting around the single bonds, and are subject to fluctuating forces from the heat bath. Such a rotational degree of freedom of partial moieties may reduce the electronic dephasing time. It is possible, therefore, that there exists a correlation between the librational motion of partial moieties and the dephasing time.

Comparison between Anthracene Dimers and Binaphthyl: Hochstrasser and his co-workers[12] reported the coherent excitation transfer in 2,2′-binaphthyl in different solvents at room temperature. The transient absorption anisotropy decay in CCl_4 exhibited a damped oscillation with a time period of 1.2 ps and a damping time constant of 180 fs. They found from the theoretical analysis that the anisotropy oscillation arises from the energy transfer recurrence among two naphthyl moieties associated with $2\beta = 40$ cm^{-1} and $T_2' = 0.18$ ps (Table 2). Comparing the case of binaphthyl with the present cases of anthracene dimers, one can see that the dephasing time is longer in anthracene dimers by a factor of 3–6 than that in binaphthyl, while the interaction energy is comparable to those in *m*-DAB and DTA. It is considered that the dimeric structure in binaphthyl is much more flexible than in *m*-DAB from a comparison of the molecular sizes of the two molecules, and is thus subject to fluctuating forces. This may greatly reduce the electronic dephasing time in the case of binaphthyl.

Consequently, the longer dephasing time in anthracene dimers is predominantly responsible for the appearance of excitation recurrence. In fact, the rapid librational motion of naphthalene rings in binaphthyl may cause the shortest dephasing time of 0.18 ps. This makes also a striking contrast between the anthracene dimers and binaphthyl with respect to the key parameter for the coherent dynamics $2\beta T_2'$. The $2\beta T_2'$ values in the anthracene dimers (5.0–19,0) are much larger than unity, whereas the value is close to unity in binaphthyl (1.4).

5.3 Solvent Effects. The results of *m*-DAB show that the oscillation frequency in $r(t)$ curve is different in the two solvents (Figs. 6 and 7); $\omega_{osc} = 6.9 \times 10^{12}$ rad·s^{-1} in toluene and 11.4×10^{12} rad·s^{-1} in THF. This difference results in a fairly large difference in the interaction energy β according to Eq. 6; $\beta = 18.7$ cm^{-1} in toluene and 30.5 cm^{-1} in THF (Table 2). It is rather surprising that the intramolecular parameter shows such a large dependence on solvents. Note that the magnitude of β is sensitive to a change in the dimer conformation, it follows that the chromophores are much more mobile in THF than in toluene to take a dimer conformation preferable to the interchromophore interaction. This view is consistent with an experimental result that the rotational diffusion rate estimated from the $r(t)$ curve is faster in THF (50 ps) than in toluene (87 ps) (Table 1), although the macroscopic solvent viscosity is similar each other ($\eta = 0.460$ in THF and 0.552 in toluene at 25 °C). The related study for binaphthyl[12] shows also a solvent effect on the oscillatory behaviors; $\omega_{osc} = 5.3 \times 10^{12}$ rad·s^{-1} in CCl_4 and $\omega_{osc} = 2.2 \times 10^{12}$ rad·s^{-1} in hexane. In this case, the interaction energy is similar with each other since T_2' is different between the two solvents ($T_2' = 0.18$ ps in CCl_4 and 0.14 ps in hexane). At present, the solvent effect

on oscillatory behaviors remains unsettled. Clearly further studies are required before a fully consistent picture is available for the solvent effect.

6. Concluding Remarks

We have observed the quantum coherence associated with exciton migration in bichromophoric molecules in condensed phase. For several types of anthracene dimers in solution at room temperature, the damped oscillations were observed on the fluorescence anisotropy decays in the short time region <3 ps, and were analyzed in terms of a scheme of the recurrence motion of an excitation between coupled chromophores. From the analyses based on the theoretical formula developed by Wynne and Hochstrasser,[18–20] the exciton interaction energy and the pure dephasing time were evaluated. The magnitudes of interaction energy ($2\beta = 30$–100 cm^{-1}) imply substantial contribution from the electron exchange interaction in addition to the dipole–dipole resonance interaction. The damping time constants for molecules having rigid dimer structures (*o*-DAB and DTA) are significantly longer than those of *m*-DAB and binaphthyl. Such a fairly slow dephasing time can be regarded as due to a rigid and fixed dimeric conformation.

The interpretation for the anisotropy decay remains unsolved. The observed $r(t)$ curves do not fit with the theoretical ones at early times <0.2 ps, particularly in *o*-DAB. This discrepancy might be attributed to a fast depolarizing process like internal vibrational redistribution being involved besides the dominant coherent process. In the case of DTA, the $r(t)$ curve starts from a negative value, contrary to the case where the transition dipole moments for absorption and fluorescence are identical and $r(0) = +0.7$. The negative value at $t = 0$ has been explained in terms of an additional contribution from another fluorescent component due to a vibronic transition with a nontotally symmetric vibration.

The present study provides additional examples of the coherent energy transfer dynamics in organized molecular systems. Particularly, the present study demonstrates that a rigid and fixed conformation of reacting chromophores plays an important role in reducing the electronic dephasing rate, and in leading the molecular system into the underdamped condition $2\beta T_2' > 1$. Further experimental studies on the coherent energy transfer will be presented in a forthcoming paper for another type of dimeric structure of anthracene chromophores. As future work along this line, it would be interesting to investigate the effect of breaking the site-energy degeneracy of the chromophores by adding various substituent groups to one of them.

The present work was supported by Grant-in-Aid for Scientific Research on Priority Areas (B) (No. 11223203) from the Ministry of Education, Culture, Sports, Science and Technology. The authors (IY and SA) acknowledge Prof. Yoshiteru Sakata (Osaka University) for his collaboration with us in offering oppotunities to test the coherent dynamics for many kinds of anthracenophane compounds which were synthesized by his research groups.

References

1 I. Yamazaki, S. Akimoto, T. Yamazaki, H. Shiratori, and A. Osuka, *Acta Phys. Pol.*, **95**, 105 (1999).

2 A. Nakano, A. Osuka, T. Yamazaki, Y. Nishimura, S. Akimoto, I. Yamazaki, A. Itaya, M. Murakami, and H. Miyasaka, *Chem.—Eur. J.*, **7**, 3134 (2001).

3 M. S. Choi, T. Yamazaki, I. Yamazaki, and T. Aida, *Angew. Chem., Int. Ed.*, **43**, 150 (2004).

4 Th. Förster, "Modern Quantum Chemistry, Part III, Action of Light and Organic Crystal," ed by O. Sinanoglu, Academic Press, New York (1965), pp. 93–137.

5 D. C. Arnett, C. C. Moser, P. L. Dutton, and N. F. Scherer, *J. Phys. Chem. B*, **103**, 2014 (1999).

6 H. Sumi, *Chem. Rec.*, **1**, 480 (2001).

7 G. R. Fleming and R. van Grondelle, *Phys. Today*, **47**, 48 (1994).

8 T. S. Rahman, R. S. Knox, and V. M. Kenkre, *Chem. Phys.*, **44**, 197 (1979).

9 R. S. Knox and D. Gülen, *Photochem. Photobiol.*, **57**, 40 (1993).

10 A. Matro and J. A. Cina, *J. Phys. Chem.*, **99**, 2568 (1995).

11 T. Kato and Y. Fujimura, *Chem. Phys. Lett.*, **202**, 95 (1996).

12 F. Zhu, C. Galli, and R. M. Hochstrasser, *J. Chem. Phys.*, **98**, 1042 (1993).

13 I. Yamazaki, S. Akimoto, T. Yamazaki, S. Sato, and Y. Sakata, *J. Phys. Chem. A*, **106**, 2122 (2002).

14 I. Yamazaki, N. Aratani, S. Akimoto, T. Yamazaki, and A. Osuka, *J. Am. Chem. Soc.*, **125**, 7192 (2003).

15 I. Yamazaki, N. Tamai, and T. Yamazaki, *J. Phys. Chem.*, **94**, 516 (1990).

16 S. Akimoto, I. Yamazaki, T. Sakawa, and M. Mimuro, *J. Phys. Chem. A*, **106**, 2237 (2002).

17 L. Allen and J. H. Eberly, "Optical Resonance and Two-level Atoms," Wiley-Interscience, New York (1975).

18 K. Wynne and R. M. Hochstrasser, *Chem. Phys.*, **171**, 179 (1993).

19 K. Wynne, S. Gnanakaran, C. Galli, F. Zhu, and R. M. Hochstrasser, *J. Lumin.*, **60/61**, 735 (1994).

20 K. Wynne and R. M. Hochstrasser, *J. Raman Spectrosc.*, **26**, 561 (1995).

21 M. Kuritani, Y. Sakata, F. Ogura, and M. Nakagawa, *Bull. Chem. Soc. Jpn.*, **46**, 605 (1973).

22 Y. Sakata, T. Toyoda, T. Yamazaki, and I. Yamazaki, *Tetrahedron Lett.*, **33**, 5077 (1992).

23 a) M. J. S. Dewar, E. G. Coebisch, E. F. Healy, and J. J. P. Stewart, *J. Am. Chem. Soc.*, **107**, 3902 (1985). b) J. J. P. Stewart, "MOPAC 93.0 Manual," Fujitsu Limited, Tokyo (1993).

24 J. N. Murrell and J. Tanaka, *Mol. Phys.*, **7**, 363 (1964).

25 S. Sato, Y. Nishimura, Y. Sakata, and I. Yamazaki, *J. Phys. Chem. A*, **107**, 10019 (2003).

Iwao Yamazaki was born in 1942 in Sapporo. He received his Ph. D degree in 1972 from Hokkaido University on Molecular Photophysics, and then joined Hokkaido University as an Assistant Professor. In 1980, he moved to the Institute for Molecular Science (Okazaki, Japan) as an Associate Professor, and then joined Hokkaido University in 1988 as a Full Professor at the Department of Chemistry. His research interest is ultrafast photochemical processes in organized molecular systems and their applications to quantum mechanical processors. In 1990 he received the Distinguished Research Award, Chemical Society of Japan in the field of time-resolved spectroscopy of molecular photophysics.

Seiji Akimoto was born in 1964 in Osaka. He graduated Kyoto University in 1988 and received his Ph. D degree from Kyoto University in 1994. During 1992–1993, he was a Research Fellow of the Japan Society for the Promotion of Science for Young Scientists. In 1993, he joined Hokkaido University as Assistant Professor. His research interest is excited-state dynamics of organic molecules in biological systems and artificial molecular systems.

Naoki Aratani was born in 1975 in Nagoya. He received his B.Sc and M.Sc degrees in 1999 and 2001, respectively, from Kyoto University. He became a fellow of Japan Society for the Promotion of Science (JSPS) in 2001, and is currently Assistant Professor of Kyoto University. His research interest directs towards exploration of functional giant porphyrin arrays.

Atsuhiro Osuka was born in Gamagori, Aichi in 1954. He received his Ph. D degree from Kyoto University in 1982 on photochemistry of epoxyquinones. In 1979, he started an academic career at Department of Chemistry of Ehime University as Assistant Professor. In 1984, he moved to Department of Chemistry of Kyoto University, where he became a professor of chemistry in 1996. He was awarded the CSJS Award for Young Chemists in 1988 and the Japanese Photochemistry Association Award in 1999. His research interests cover many aspects of synthetic approaches toward artificial photosynthesis and development of porphyrin-related compounds with novel structures and functions.